

## 3D FREQUENCY SELECTIVE SURFACES

S. N. Azemi\*, K. Ghorbani, and W. S. T. Rowe

School of Electrical and Computer Engineering, RMIT University,  
GPO Box 2476, Melbourne, VIC 3001, Australia

**Abstract**—A novel 3D Frequency Selective Surface (FSS) architecture based on a circular ring unit element is presented. The circular ring was made 3D by creating a cylindrical element of a certain length, adding an extra degree of freedom into the structure. The length of the cylinder is shown through electromagnetic simulation to have a significant effect on the frequency characteristics of the FSS. Increasing the length of the cylinder can change the FSS from a band-stop to a band-pass filter response. The center frequency of both band pass and band stop responses can also be tuned with adjustment to the length. Dielectric materials are introduced in the center of the cylindrical unit cell elements to simultaneously obtain a stop and pass band with a sharp transition. For high dielectric filling materials, the 3D periodic structure exhibits negative refractive index metamaterial properties. A parametric analysis was conducted on these new cylindrical unit elements, and a prototype 3D FSS structure has been constructed and experimentally validated.

### 1. INTRODUCTION

Frequency Selective Surfaces (FSSs) have been receiving increased interest in various communication systems applications. FSSs are periodic resonant structures that behave like a spatial filter. The FSS can either block or pass electromagnetic waves of a certain frequency depending on its specific shape or structure. Numerous different resonant shapes have been used for FSS design, for example a circle [1], square [2], hexagon [3] and fractal geometries [4, 5]. An FSS can be designed to function with a high-pass, low-pass, band stop or band pass filter response.

A wide variety of methods can be found in the literature for improving the characteristics of traditional 2D FSSs. One trend is

---

*Received 30 March 2012, Accepted 9 May 2012, Scheduled 22 May 2012*

\* Corresponding author: Saidatul Norlyana Azemi (snorlyana@yahoo.com).

to implement a tuning circuit as part of the FSS pattern so that the frequency properties can be varied [6]. High frequency PIN diodes are commonly used to switch on or off sections of the pattern, thus making the surface inductive or capacitive. Another technique is by adjusting the DC voltage applied to a varactor to modify the reflectivity and transmissivity of a FSS. However, these tunable circuit FSSs employ a huge number of active elements, which can increase the size, cost, and complexity of the design.

FSSs with very close band of operation have also been reported recently [7]. When narrow frequency band separation is desirable a multiband FSS can be constructed using concentric double square elements [8]. The band separation is proportional to the gap between concentric elements. Consequently, strict fabrication tolerances are required, and the coupling between the concentric elements difficult to control. A gridded square FSS has also been proposed to yield closer reflection/transmission band ratios of 1.3 to 2.1 compared to greater than 2.5 for the single square FSS [9, 10]. This approach requires a multilayer structure which adds to the complexity and cost of the fabrication.

Multi-layered FSS architectures have also been used to address other shortcomings of conventional FSSs. For instance, a 2D FSS can be sandwiched or stacked between thick dielectric materials in order to obtain multi-band response [11, 12]. Varying the separation width or thickness of dielectric, maximally flat or multiple responses can be obtained. Recently, a 2D periodic array of multimode cavities/resonators was demonstrated [11] offering greater flexibility in terms of controlling the number and position of desired transmission poles and zeros. The cavity modes and coupling can be controlled in order to obtain a desired frequency response. Moreover, 3D FSSs [13] can also offer greater flexibility and extra control providing an extra degree of freedom when compared to a conventional 2D FSS where the design limitations are relatively well known [14].

In this paper, we propose and investigate 3D cylindrical FSS architectures. The 3D FSS consists of vertically arranged cylindrical unit elements of a certain length, extending the potential functionality of the structure beyond that of its 2D analogue, a circular ring FSS. By varying the length of the 3D cylindrical FSS, the frequency response can be tuned, as well as producing either band pass or band stop operation. A parametric analysis of the 3D FSS cylindrical elements is undertaken using CST electromagnetic software, and experimental validation is attained. In addition, a study in to the effect of dielectric materials introduced in the center of the 3D cylindrical FSS unit cell architecture is also presented. The addition of the dielectric filling can

significantly modify the frequency response providing greater design flexibility, and the ability to achieve an extremely closely spaced stop and pass band.

## 2. CIRCULAR RING FSS

A 2D circular ring resonator element provides the basis for this investigation. A conventional 2D FSS was created by periodically arraying aluminum circular ring elements on top of a 10 mm thick of foam substrate. The circular ring resonator was chosen since it has been demonstrated less sensitivity to incident wave angle than other shaped elements [15]. A schematic of the FSS is shown in Fig. 1(a). The diameter of the ring is determined using the basic ring resonator equation:  $d \approx \lambda_0/\pi$ . The diameter  $d$  of the rings and width  $w$  ( $d_{\text{outer}} - d_{\text{inner}} = 32 \text{ mm} - 29.4 \text{ mm}$ ) of the conducting strip primarily determine the location of the resonant frequency, while separation period  $s$  controls the FSS angular performance. These are general rules of thumb for designing an FSS [14, 15]. Studies have

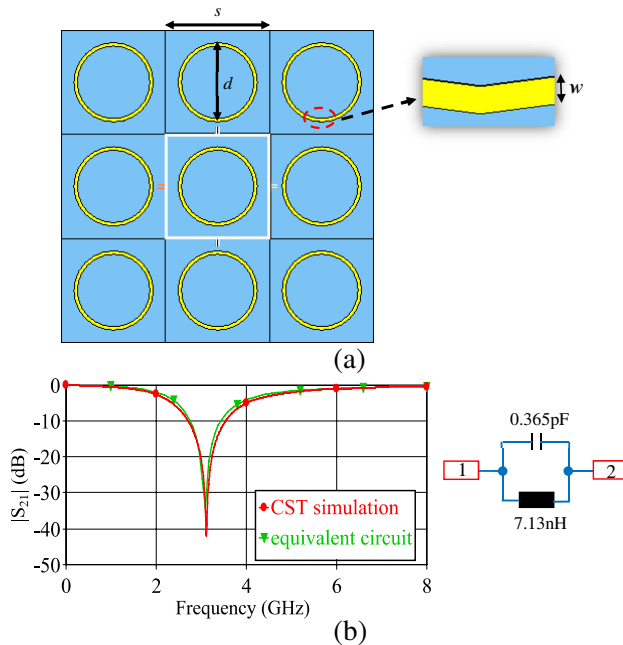


**Figure 1.** (a) Circular ring FSS — dimensions:  $s = 34 \text{ mm}$ ,  $w = 1.3 \text{ mm}$ ,  $d = 32 \text{ mm}$ . (b) Transmission and equivalent circuit of the circular ring FSS shown in (a).

shown that a smaller diameter results in a higher frequency and a smaller  $s$  ensures frequency stability with varying incident angles [15].

Figure 1(b) shows the circular ring FSS frequency response and equivalent circuit as obtained from an electromagnetic simulation in CST Microwave Studio. The simulation shows that the FSS has the expected band stop characteristic centered at 3.12 GHz. The value of inductance ( $L = 7.13$  nH) and capacitance ( $C = 0.365$  pF) is retrieved by using the following equations [16]:

$$L(\text{nH}) = 3.937 \frac{a^2}{8a + 11c} \times K_g \quad (1)$$

$$a = \frac{D_{\text{outer}} + D_{\text{inner}}}{4}$$

$$c = \frac{D_{\text{outer}} - D_{\text{inner}}}{2}$$

$$K_g = 0.57 - 0.145 \ln \frac{w}{h} \quad \text{for} \quad \frac{w}{h} > 0.05; \quad \text{where } h = 0.035 \text{ mm}$$

$$C(\text{pF}) = \frac{1}{(f \cdot 2\pi)^2} \times \frac{1}{L} \quad (2)$$

### 3. 3D CYLINDRICAL FSS

The circular ring FSS was made 3D by introducing a certain height to the conductors of the unit elements, creating cylinders with a length  $l$  (seen in Fig. 2). The desired operating frequency of this 3D cylindrical FSS can be obtained by varying the length of the resulting cylinders. Shown in Fig. 3 is the transmission results of the 3D cylindrical FSS with different lengths (all other parameters are equivalent to those in Fig. 2).

By changing the length of the cylindrical unit elements to 5 mm, 12 mm, 16 mm and 18 mm as shown in Fig. 3(a), the center of the stop band shifted to 3.2 GHz, 3.8 GHz, 4.2 GHz, and 4.7 GHz respectively. This frequency shift initially occurs without substantially affecting the stop band characteristics. The transmission minima and bandwidth obtained from the  $|S_{21}|$  curves are reasonably well maintained until the 18 mm length is reached. At this point a significant depth to the structure has been introduced, instigating a transition from a band stop to a band pass topology for the FSS. As seen in Fig. 3(b), the FSS creates a band pass characteristic at approximately 6.2 GHz as the length ( $l$ ) of the cylinder increases to 20 mm. Further increasing the length to 24 mm 30 mm and 40 mm, the center of this pass band decreases in frequency to approximately 5.4 GHz, 4.4 GHz and 3.4 GHz respectively.

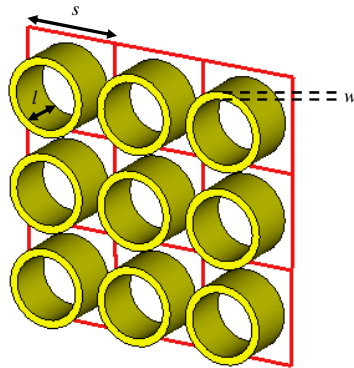


**Figure 2.** 3D cylindrical FSS —  $s = 34$  mm,  $w = 1.3$  mm,  $d = 32$  mm.

The 3D cylindrical FSS can be shown to cycle between band stop and band pass performance at a particular frequency as the length is increased. Focusing on 3.12 GHz, the frequency of the circular ring FSS stop band, Fig. 3(c) shows the 3D cylindrical FSS becomes band pass at lengths of 44.5 mm and 92 mm, whilst at an intermediate length of 68.5 mm returns to being band stop. Furthermore at 92 mm length, multiple pass bands can be seen between 1 and 5 GHz. The sequential pass or stop bands create a higher quality factor results thus the bandwidth is reduced. Thus, the characteristic response for a particular FSS geometry can be switched by varying the length of the cylinder in the 3D FSS.

Figure 4 shows the surface current density illustrating an increased number of maxima as the length of the cylinder is increased. Band pass responses shows an odd number of maxima and minima in the current density, while band stop responses show an even number. Band pass responses also correspond roughly to lengths of a half multiple of the free space wavelength, with band stop being in between.

The 3D FSS composed of metallic cylinders exhibits a resonant behaviour which can be described by the LC circuit shown in the inset to Fig. 5. For cylinders of very short length ( $l \approx 0$ ), the 3D cylindrical FSS exhibits a stop band response, resonating at a frequency of  $f = 1/(2\sqrt{L_1C_1})$ , where  $L_1$  and  $C_1$  are the equivalent inductance and capacitance of the circular ring geometry.  $L_1$  mainly depends on the diameter  $d$  of the ring, and the resonant frequency of the element can be control by adjusting  $d$ . However in this case,  $d$  is fixed. When the value of  $l$  is increased, a series inductance  $L_2$  along the cylinder begins to modify the behavior of the element. The band stop center frequency is tuned to a higher value with increasing  $l$ , until

eventually  $L_2$  dominates and generates a band pass resonance. This explains the transformation from band stop to band pass for the 3D cylindrical FSS. Consequently, the equivalent circuit becomes parallel-series when  $L_2$  becomes dominant. The equivalent circuit model was

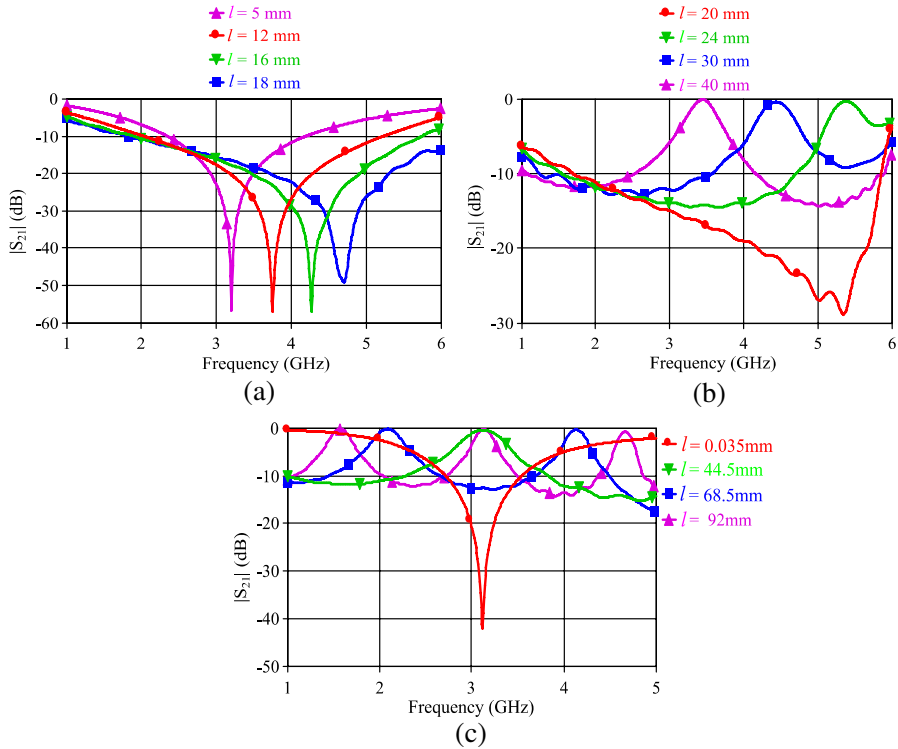


**Figure 3.** 3D cylindrical FSS transmission ( $|S_{21}|$  dB) with varied length  $l$ . (a) Center of the stop band shifted as the length is increased. (b) Transition from a band stop to a band pass after a certain length is reached. (c) 3D cylindrical FSS can cycle between band stop and band pass performance as the length is increased.

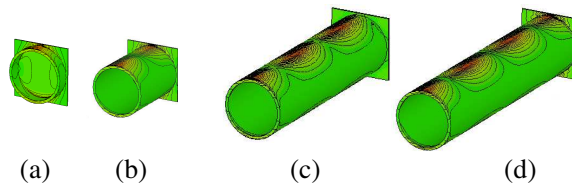


**Figure 4.** Surface current of cylindrical FSSs of different lengths (a) 5 mm, (b) 44.5 mm  $\cong \lambda_0/2$ , (c) 68.5 mm  $\cong 3\lambda_0/4$ , (d) 92 mm  $\cong \lambda_0$ .

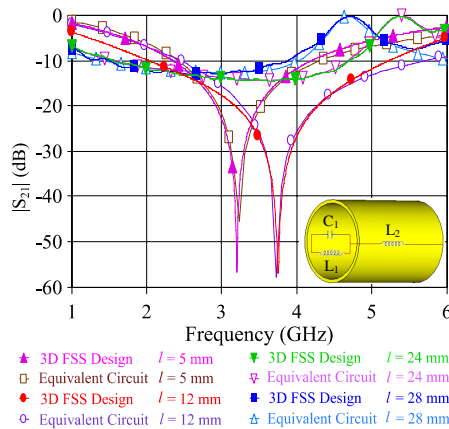


**Figure 5.** Simulated and equivalent circuit transmission results for the 3D cylindrical FSS — inset: Equivalent circuit model.

validated through comparison to the CST simulations as depicted in Fig. 5. The value of inductance  $L_2$  can be retrieved by using the following equation [17]:

$$L_2 = \frac{\mu_0}{2\pi} \left( \ln \frac{2l}{r} - 1 \right), \quad l \gg r \quad (3)$$

where  $r$  is the radius of the cylinder.

A prototype was fabricated using a cylinder length of 44.5 mm to produce a band pass response at 3.12 GHz, and was measured in free space measurement setup as shown in Fig. 6(a). For the free space measurement, the two horn antennas are placed  $\sim 50$  cm from each side of the FSS. The setup is calibrated using a flat metal diffraction plate that is the same size as the prototype. The 3D cylindrical FSS prototype is then placed in the fixture and the transmission properties are measured. Fig. 6(b) shows the comparison between the simulated and measured transmission of the 3D cylindrical FSS. Excellent agreement between simulation and measurement results was achieved, particularly in the vicinity of the pass band.

#### 4. DIELECTRIC FILLING OF THE CYLINDRICAL UNIT ELEMENTS

To highlight the potential functionality and flexibility of the 3D cylindrical FSS, a dielectric material was inserted inside the cylindrical FSS unit elements (Fig. 7). The introduction of the dielectric material enables an independent variation of the stop and pass band properties of the FSS. A very closely spaced band pass and band stop response is

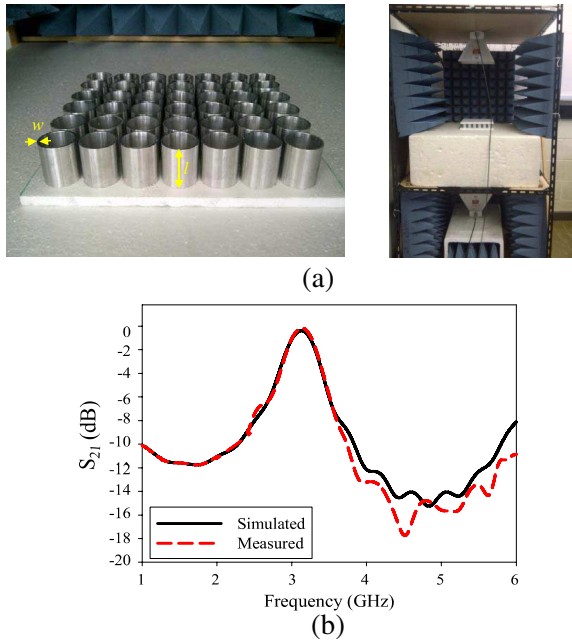


**Figure 6.** (a) Fabricated 3D FSS and the test setup —  $s = 34$  mm,  $w = 1.3$  mm,  $l = 44.5$  mm, (b) 3D FSS simulated and measured transmission response.

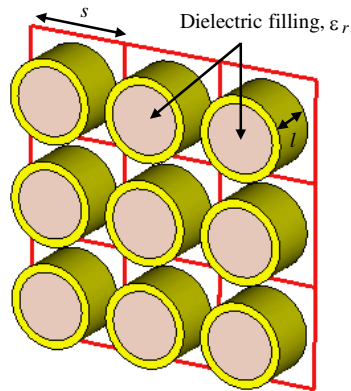


**Figure 7.** 3D Cylindrical FSS with dielectric filling —  $s = 34$  mm,  $w = 1.3$  mm,  $l = 18$  mm.

obtained in the dielectric filled FSS structure. The resonant frequency is also reduced, and with high permittivity filling materials the unit cell becomes much smaller than a free space wavelength, essentially giving it metamaterial properties.

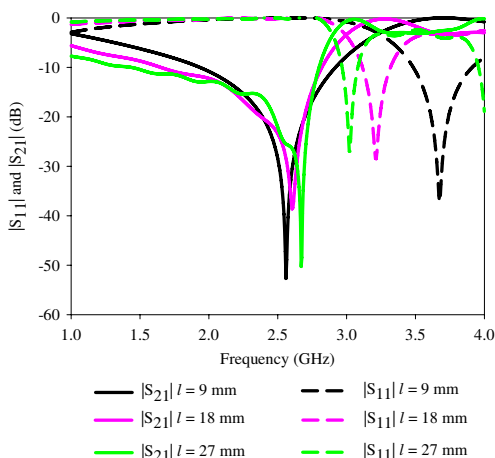


**Figure 8.**  $S$ -parameters of the 3D cylindrical FSS with different length  $l$ , using a dielectric filling  $\epsilon_r = 5$ .

The structure in Fig. 7 was simulated for different cylinder lengths with a filler material of  $\epsilon_r = 5$ . As shown in Fig. 8, the dielectric loading shifted the band stop region to a lower frequency (in the range of 2.56 GHz–2.67 GHz), and a band pass response (with minimum  $|S_{11}|$ ) is also created below 4 GHz. Similar to the previous study of different length FSS cylinders without dielectric filling in Section 3, the band stop frequency marginally increases with increasing  $l$ . However, the pass band response rapidly shifts lower in frequency for larger values of  $l$ . Partial dielectric filling the cylindrical unit cells sees the band stop response shifted to a lower frequency when the amount of dielectric in the cylinders length is increased. However, a well formed pass band (with  $|S_{11}| < -10$  dB) only occurs when the cylinders are greater than 50% full. Close band spacing between band pass and band stop is only achieved when the cylindrical elements are essentially fully filled with the dielectric material.

With the placement of a dielectric filling of  $\epsilon_r = 5$  inside each unit cell, the band stop region of the 3D cylindrical FSS in Fig. 7 shifts to a lower frequency of approximately 2.6 GHz (from 4.7 GHz for  $\epsilon_r = 1$ ), as depicted in Fig. 9. A band pass response is also seen at 3.2 GHz. Using higher dielectric value filling inside the cylinder (also seen in Fig. 9) creates sharp band responses that are very closely spaced in frequency. A detailed investigation of the influence of the dielectric filling is shown in Table 1, including the band pass to band stop ratio. Transmission/Reflection band ratios down to 1.05 are achieved. These ratios are an impressive result compared to greater than 1.3 for a gridded square FSS [7] and more than 2.5 single square FSS [9], and

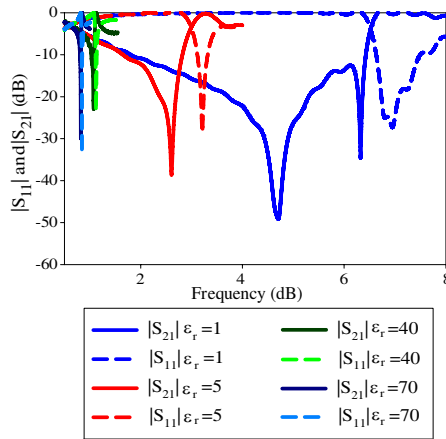


**Figure 9.** 3D Cylindrical FSS for different dielectric fillings,  $\epsilon_r$ .

**Table 1.** 3D FSS Stop and Pass Band characteristics as the dielectric filling  $\epsilon_r$  was changed.

$\epsilon_r$	Band stop frequency (GHz)	Band stop $ S_{21} $ (dB)	Band pass frequency (GHz)	Band Pass $ S_{11} $ (dB)	Frequency Ratio (band pass/band stop)
1	4.74	-49.9	7.0	-28.2	1.48
5	2.61	-38.8	3.22	-27.4	1.23
10	1.96	-36.7	2.24	-25.5	1.14
20	1.45	-33.2	1.58	-29.5	1.09
30	1.19	-26.7	1.3	-34.2	1.09
40	1.05	-24.7	1.13	-22.6	1.08
50	0.93	-37.2	1.0	-17.6	1.08
60	0.86	-22.6	0.93	-15.1	1.08
70	0.77	-16.2	0.83	-12.2	1.08
80	0.74	-12.6	0.79	-10.6	1.07
90	0.71	-11.6	0.75	-10.1	1.06
100	0.64	-8.61	0.68	-8.61	1.06
120	0.61	-7.84	0.64	-8.6	1.05

comparable to [10]. It should be noted however that as the dielectric value is increased beyond  $\epsilon_r \approx 70$  the  $s$ -parameter dip magnitudes deteriorate.

The effective electrical size of the 3D Cylindrical FSS unit cell

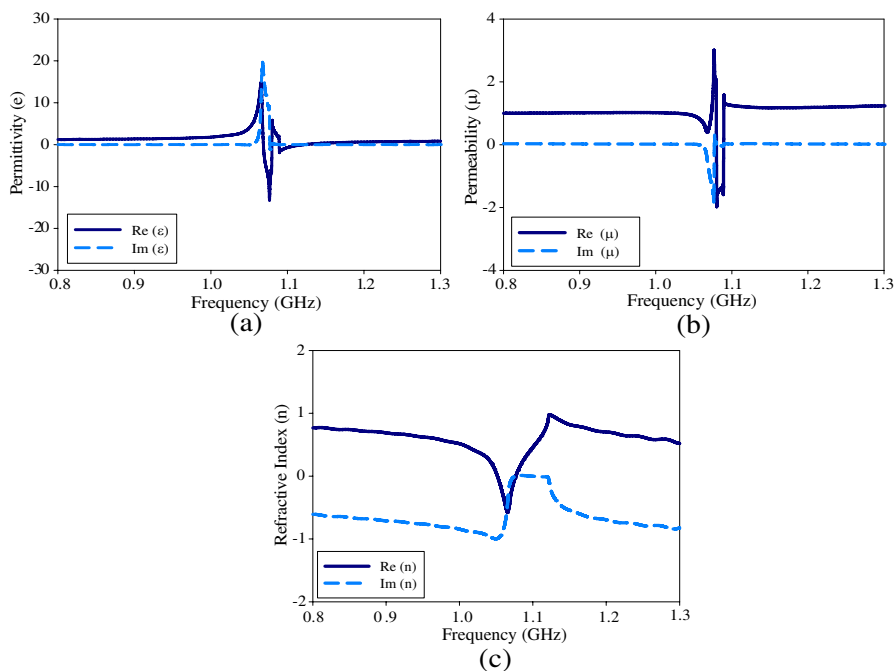


**Figure 10.** (a) Effective permittivity. (b) Effective permeability. (c) Refractive index for a 3D cylindrical FSS with dielectric filling  $\epsilon_r = 40$ .

becomes a fraction of a free space wavelength (less than  $\lambda_0/8$  is used here) for dielectric fillings with  $\epsilon_r > 40$ , allowing bulk metamaterial properties to be extracted. Shown in Fig. 10 are the effective permittivity, permeability and refractive index that are retrieved from simulations of a 3D cylindrical FSS with a dielectric filling of  $\epsilon_r = 40$  (using the macro available in the CST software). Figs. 10(a) and (b) show that the real part of the effective permittivity and permeability are negative at approximately 1.08 GHz. Moreover, the refractive index in Fig10. (c) confirms that a negative refractive index band lies in the same vicinity. This negative index is achieved with a single uniform unit cell structure, as compared to the binary unit cells used in [18].

## 5. CONCLUSION

In this paper a new type of frequency selective surface based on a 3D cylindrical unit element is described. As height is added to the conducting elements of a circular ring FSS (length of cylinders), the stop band response is shifted to a higher frequency. The transmission

minima and bandwidth are reasonably well maintained. At a certain length for a particular operating frequency the FSS changes from band stop to band pass, and continues to cycle between these responses with increased length. The simulated FSS properties were validated through an equivalent circuit model as well as experimental results, both of which showed very good agreement.

A close transmission/reflection band separation can be obtained through inserting a dielectric filling inside the cylindrical unit cell structure of the 3D FSS. For a dielectric filling with  $\epsilon_r > 40$  the effective electrical size of the unit cell was sufficiently reduced to enable the analysis of the bulk metamaterial properties, which exhibited a negative refractive index band.

The structures in this paper lend themselves to high aspect ratio micro-fabrication techniques for efficient implementation at higher frequencies. The 3D FSS exhibits tremendous potential in alleviating the limitations of 2D FSSs, and offering potential functionality beyond the capabilities of its 2D analogue. Further explorations into the properties of 3D FSS structures (including their angular stability) will be the subject of future work.

## REFERENCES

1. Taylor, P. S., J. C. Bathelor, and E. A. Parker, "A passively switched dual-band circular FSS slot array," *IEEE Conference on Antenna and Propagation in Wireless Communications (APWC)*, 648–651, 2011.
2. Li, L., C. Qiang, Y. Qiaowei, K. Sawaya, T. Maruyama, T. Furuno, and S. Uebayashi, "Frequency selective reflect array using crossed-dipole element with square loops for wireless communication applications," *IEEE Transactions on Antennas and Propagation*, Vol. 59, No. 1, 89–99, 2011.
3. Zheng, S. F., Y. Z. Yin, and X. S. Ren, "Interdigitated hexagon loop unit cells for wideband miniaturized frequency selective surface," *9th International Symposium Antennas Propagation and EM Theory (ISAPE)*, 770–720, 2010.
4. Xue, J.-Y., S.-X. Gong, P.-F. Zhang, W. Wang, and F.-F. Zhang, "A new miniaturized fractal frequency selective surface with excellent angular stability," *Progress In Electromagnetics Research Letters*, Vol. 13, 131–138, 2010.
5. Zhang, J.-C., Y.-Z. Yin, and J.-P. Ma, "Frequency selective surfaces with fractal four legged elements," *Progress In Electromagnetics Research Letters*, Vol. 8, 1–8, 2009.

6. Ucar, M. H. B., A. Sondas, and Y. E. Erdemli, "Switchable splitting frequency selective surfaces," *Progress In Electromagnetics Research B*, Vol. 6, 65–79, 2008.
7. Al-Joumayly, M. and N. Behdad, "Low-profile, highly-selective, dual-band frequency selective surfaces with closely spaced bands of operation," *IEEE Transactions on Antennas and Propagation*, Vol. 58, No. 12, 4045–4050, 2010.
8. Langley, R. J. and E. A. Parker, "Double-square frequency selective surface and their equivalent circuit," *Electronic Letters*, Vol. 19, No. 17, 675–677, 1983.
9. Wang, Z. L., K. Hashimoto, N. Shinohara, and H. Mastsumoto, "Frequency selective surface for power transmission," *IEEE Trans. on Microwave Theory and Techniques*, Vol. 47, No. 10, 2039–2042, 1999.
10. Qing, A. and C. K. Lee, "Analysis of gridded square frequency selective surfaces," *Asia Pacific Microwave Conference (APMC)*, 58–61, 2000.
11. Rashid, K. and Z. Shen, "Three-dimensional monolithic frequency selective structure with dielectric loading," *Asia-Pacific Microwave Conference Proceedings (APMC)*, 873–876, 2010.
12. Teo, P. T., X. F. Luo, and C. K. Lee, "Frequency-Selective Surfaces for GPS and DCS1800 mobile communication, Part 1: Quad-layer and single-layer FSS design," *IET Microwaves, Antenna Propagation*, Vol. 1, No. 2, 2007.
13. Azemi, S. N. and W. S. T. Rowe, "Development and analysis of 3d frequency selective surfaces," *Asia Pacific Microwave Conference (APMC)*, 693–696, 2011.
14. Munk, B. A., *Frequency Selective Surface: Theory and Design*, Wiley-Interscience, New York, 2000.
15. Huang, J., W. T. Kao, and S. W. Lee, "Tri-band frequency selective surface with circular ring elements," *IEEE Transactions on Antennas and Propagation*, Vol. 42, No. 2, 166–175, 1994.
16. Hong, J. S., and M. J. Lancaster, *Microstrip Filters for RF/Microwave Applications*, Wiley-Interscience, New York, 2001.
17. Karmel, P. R., G. D. Colef, and R. L. Camisa, *Introduction to Electromagnetic and Microwave Engineering*, John Wiley & Sons, 1998.
18. Wang, J. F., S. B. Qu, H. Ma, Y. M. Yang, and X. Wu, "Wide-angle polarization-independent planar left handed metamaterials based on dielectric resonators," *Progress In Electromagnetics Research B*, Vol. 12, 243–258, 2009.